Vietnam Journal of Science and Technology ***62*** *(1) (2024) 78-91*

doi:10.15625/2525-2518/17531

Preparation of expandable flake-graphites with different particle sizes and their flame-retardant application for polypropylene

Nhung Hac Thi[1, 2], Thi Thu Hien Nguyen[1], Truong Cong Doanh[3], Do Thi Mai Huong[4], Tien Dat Doan[1, 2], Ho Thi Oanh[1], Nguyen Duc Tuyen[1], Mai Ha Hoang[1, 2, *]

[1]*Institute of Chemistry, Vietnam Academy of Science and Technology, 18 Hoang Quoc Viet, Cau Giay, Ha Noi, Viet Nam*

[2]*Graduate University of Science and Technology, Vietnam Academy of Science and Technology, 18 Hoang Quoc Viet, Cau Giay, Ha Noi, Viet Nam*

[3]*Hanoi University of Industry, 298 Cau Dien, Bac Tu Liem, Ha Noi, Viet Nam*

[4]*University of Fire Prevention and Fighting, 243 Khuat Duy Tien, Thanh Xuan, Ha Noi, Viet Nam*

[*]Emails*: hoangmaiha@ich.vast.vn*

Received: 21 September 2022; Accepted for publication: 26 November 2022

Abstract. Bisulfate intercalated graphites with different particle sizes were prepared by a chemically oxidative method using natural flaky graphites as raw materials. The morphology and structure of the expandable graphites were confirmed by Fourier transform infrared spectroscopy, X-ray diffraction patterns, and scanning electron microscope. The effect of the particle size on the expanded volume was also investigated. Expandable graphite with +100 mesh particle size (EG_{100}) showed the highest expanded volume of 225 mL/g. Moreover, a combination of expandable graphite, red phosphorus (RP), and melamine cyanurate (MC) into a polypropylene (PP) matrix exhibited a synergistic flame retardant effect. The composite loading EG_{100}, RP, and MC with a mass ratio of 1:1:1 and a total filler content of 18 wt.% achieved a UL94 V-0 rating and a limiting oxygen index (LOI) of 28.9 %. The effect of particle size of expandable graphite on the mechanical properties was also evaluated.

Keywords: graphite, flake-graphite, flame retardant, polypropylene.

Classification numbers: 2.5.2, 2.9.4

1. INTRODUCTION

Expandable graphite (EG), a kind of graphite intercalation compounds (GICs), was prepared by inserting intercalants between carbon sheets [1]. The weak Van der Waals interaction between flake graphite layers can be broken down by chemical or physical methods [2], while the C-C covalent bonds within the hexagonal structure of each layer can be preserved [3]. GICs possess several excellent characteristics due to their unique crystal structure [4],

including high surface area, superconductivity, and high thermal conductivity that graphite or intercalating materials do not have. Expandable graphite and expanded graphite exhibit their enormous potential for applications such as conductive, environmental adsorption, sealing, and biomedical materials [5, 6]. Expandable graphite is also considered an ideal intumescent flame retardant for polymers because of its high flame retardant efficiency, low cost, low smoke, halogen-free, and anti-dripping melt [7]. During sudden heating, the degradation and fast evaporation of intercalants or the redox reaction between those substances and the carbon of graphite produce blowing gasses propelling the adjacent graphene layers apart from each other. Consequently, the volume of EG sheets in composites extends several hundred folds, forming a char layer with worm-like structures to isolate the burning material from heat [8].

In general, GIC-bisulfate has been prepared by a chemically oxidative intercalation method employing strong oxidants (including potassium permanganate, concentrated nitric acid, potassium dichromate, chromium trioxide, etc.) and concentrated sulfuric acid [9 - 15]. Recently, some new methods have been proposed to prepare expandable graphite by adopting nitric acid [16, 17], hydrochloric acid [18], perchloric acid [19 - 21], and boric acid [22], which can introduce other pollutants or harmful reagents. The electrochemical intercalation technique has been reported to be environmentally friendly because it uses dilute acid concentrations without oxidants [23, 24]. However, the drawbacks of the method are the relatively complicated installation, low performance, and high cost.

In this work, expandable graphites with different particle sizes were synthesized by chemical oxidation using natural flaky graphites as raw materials and $KMnO_4/NH_4NO_3/H_2SO_4$ as oxidative intercalation reagents. Furthermore, high flame retardant composites based on the polypropylene (PP) matrix with the combination of expandable graphite, red phosphorus (RP), and melamine cyanurate (MC) were prepared by melt blending. The properties of the composites, including flame resistance, thermal-oxidative stability, and mechanical properties, were investigated.

2. MATERIALS AND METHODS

2.1. Materials

Natural flake graphites (particle sizes: +50, +80, +100, +150, and +200 mesh, 99 wt.% carbon basis) were provided by ACS Material, LLC. Polypropylene (advanced-PP 1102K, melt flow rate of 3.4 g/10 min, density of 0.91 g/cm^3) was bought from Advanced Petrochemical Company, Saudi Arabia. Melamine cyanurate (> 98 %), red phosphorus (≥ 97 %), and poly(methyl-hydro siloxane) (viscosity of 15-40 mPa.s (20 ºC)) were supplied by Sigma-Aldrich. $KMnO_4$, NH_4NO_3, and H_2SO_4 were of high purity and were used directly without further purification.

2.2. Synthesis of expandable graphites

Expandable graphite was prepared via a chemical oxidation method employing $KMnO_4$ as an oxidant, NH_4NO_3 as an intercalation-assisted reagent, and H_2SO_4 as both an intercalation reagent and the environment for the oxidative reaction. Firstly, 1.2 g of NH_4NO_3 and 80 mL of H_2SO_4 were combined in a beaker, and the mixture was lightly stirred. Next, 10 g of graphite was added to the mixture which was then mixed well. After that, 4.5 g of $KMnO_4$ was slowly added to the mixture, and the system was placed in a water bath at a constant temperature of 30 ºC during the process. After the addition of $KMnO_4$ was finished, the mixture was further

stirred for 10 min at a speed of 100 rpm. Afterwards, a certain amount of distilled water was dropped into the mixture to dilute the acid concentration. The solid was filtered and washed many times with distilled water until neutral. Finally, the sample was dried at 70 ºC for 12 h to obtain expandable graphite. The same procedure was applied to prepare expandable graphites (EG_{50}, EG_{80}, EG_{100}, EG_{150}, EG_{200}) using natural graphites with different particle sizes (+50, +80, +100, +150, and +200 mesh, respectively).

2.3. Surface modification of flame retardants

To improve the compatibility between melamine cyanurate/red phosphorus and the polymer matrix, those fillers were modified with poly(methyl-hydro siloxane) by dry milling method using a planetary ball mill system (Fritsch Pulverisette, Germany). The flame retardants were treated with 3 wt.% of the compatibilizer at a speed of 400 rpm for 10 min.

2.4. Preparation of flame retardant composites

Flame-retardant PP composites were prepared by melt blending in a Haake Rheomix 610 extruder at 175 ºC and a screw rate of 50 rpm for 8 min. Then, these molten mixtures were injected into a mold with a thickness of 3 ± 0.2 mm and were hot-pressed at about 200 ºC and 12 MPa for around 7 min on a Toyoseiky hot-plate compressor. Finally, the samples were naturally cooled to room temperature. The formulation of the composites is detailed in Table 1.

Table 1. The composition of the PP composites.

Sample code	Composition (wt.%)							
	PP	RP	MC	EG_{50}	EG_{80}	EG_{100}	EG_{150}	EG_{200}
PP	100	-	-	-	-	-	-	-
PP1	82	-	-	-	-	18	-	-
PP2	82	18	-	-	-	-	-	-
PP3	82	-	18	-	-	-	-	-
PP4	82	6	6	6	-	-	-	-
PP5	82	6	6	-	6	-	-	-
PP6	82	6	6	-	-	6	-	-
PP7	82	6	6	-	-	-	6	-
PP8	82	6	6	-	-	-	-	6

2.5. Characterization

Expanded volume (EV) of EG was evaluated in a temperature range of 200 - 700 ºC, and the measurement was conducted as follows: a certain amount of EG was added to a quartz beaker preheated for 5 min at tested temperatures. After that, the beaker was put into a furnace at tested temperatures until the sample was no longer expanded. Then, the volume of the samples in the quartz breaker was measured, and the EV of expandable graphites was calculated

according to equation (1). The EV of each sample at a certain temperature was determined by the average value of three measurements under the same test condition.

$$EV = V/g \quad (1)$$

where: EV is the expanded volume of EG (mL/g), V is the volume of EG after heating (mL), g is the load of EG added to the quartz beaker (g).

Vertical burning tests (UL94-V) were conducted on a horizontal and vertical flame chamber (GT-MC35F-2, Gester) following ASTM D3801-96. Limiting oxygen indexes (LOI) was obtained on an oxygen index flammability tester (Yasuda 214) corresponding to ASTM D2863-97. The dimension of the tested samples was 125 mm × 13 mm × 3 mm for both tests. The result of each sample was the average of five measurements.

Fourier transform infrared (FT-IR) spectra were recorded in the wavenumber range of 450-4000 cm^{-1} by a PerkinElmer FT-IR spectrometer. The X-ray diffraction (XRD) patterns were investigated on a D8 ADVANCE instrument (Brucker) in a 2θ range of 10-70º with Cu-K_α radiation (λ = 1.5406 Å). The field emission scanning electron microscopy (FE-SEM) micrographs of the samples were obtained by a Hitachi S-4800 system. Samples that were subjected to FT-IR, XRD, and SEM measurements included the graphite with +100 mesh particle size (FG_{100}), expandable graphite (EG_{100}), and expanded graphite (EG_{100} was heat-treated at 700 °C) (EG700 ºC). Thermogravimetric analyses (TGA) were performed using a LABSYS Evo STA system over a temperature range from ambient to 900 ºC with a heating rate of 10 ºC/min under air atmosphere. Tension tests were conducted using a Gotech Testing Machine according to ISO 527 with a tension rate of 50 mm/min. The unnotched Izod impact values were determined using TestResources following ASTM D4812. The average of five measurements was reported along with the error.

3. RESULTS AND DISCUSSION

3.1. Morphology and structure of expandable graphite

FT-IR spectra of samples FG_{100}, EG_{100}, and EG700 ºC are depicted in Figure 1a. Generally, there appear characteristic peaks of the graphite at around 1632 cm^{-1}, 1118 cm^{-1}, and 602 cm^{-1}. For expandable graphite, the FT-IR spectrum shows a new absorption peak at 1207 cm^{-1} corresponding to C=S vibrations [25], which indicates the interaction between graphite and sulfuric acid. Characteristic peaks at 1057 cm^{-1} and 870 cm^{-1} are assigned to the C-O stretching vibrations in C-OH groups and =C-H stretching vibrations [26], suggesting the formation of oxygen-containing groups on the edges and surface of the graphite after the oxidation of graphite. After heat shock, the characteristic bands of the oxygen-containing groups disappear, indicating the decomposition of those groups. Furthermore, the absorption intensity of the peaks corresponding to graphite in the FT-IR spectrum of EG700 ºC diminishes significantly, which is due to the redox reaction between the graphite and the intercalation compounds to release blown gases.

Figure 1b shows XRD patterns of the flake graphite, expandable graphite, and expanded graphite. The major diffraction peaks of natural flake graphite are at 2θ of 26.53º (d_{002} = 0.3357 nm) and 54.64º (d_{004} = 0.1678 nm) with sharp shapes and high intensities. These results indicate that the graphite possesses a high crystallization degree and a good order arrangement of graphene layers. After the treatment processes, the diffraction angle of the materials decreases slightly to 2θ = 26.41º (d = 0.3372 nm) for EG_{100} and to 2θ = 26.35º (d = 0.339 nm) for EG700 ºC, respectively.

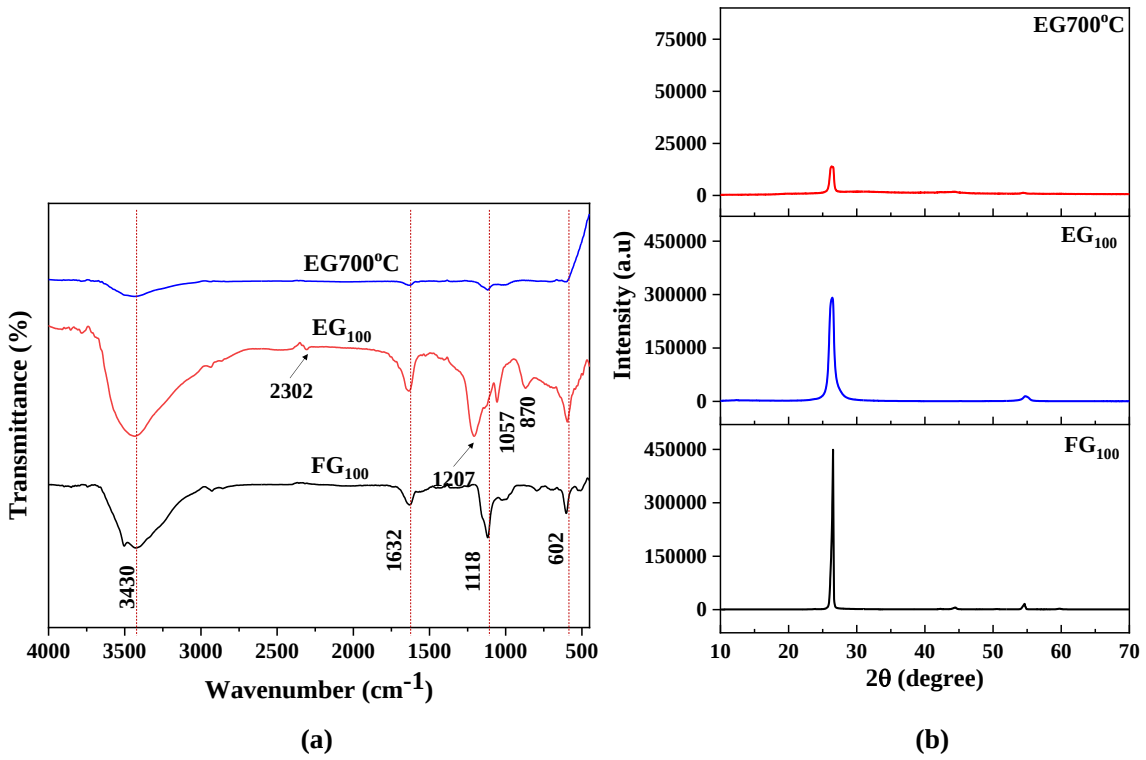

Figure 1. FTIR spectra (a) and XRD patterns (b) of FG_{100}, EG_{100}, and EG700 ºC.

In addition, the diffraction peak intensities of the expandable graphite and the expanded graphite drop considerably, and the peaks become wider. The d_{002} diffraction peak intensity ratio of FG_{100}, EG_{100}, and EG 700 ºC is 1.0000 : 0.6500 : 0.0309. After the intercalation, the graphite material is partially oxidized at the surface and edge of the carbon layers. Therefore, oxygen-containing groups are formed on the layers, and the intercalating agents are inserted into the gap between the carbon layers. As a result, the d-spacing of expandable graphite rises compared to the natural graphite. However, the intercalation process is not uniform in all layers of the graphite, leading to an increase in the disorder level of crystal structure. Consequently, the intensity of the characteristic diffraction peaks reduces, and the width of those peaks increases. After thermal treatment, the fast evaporation of propellants leads to the significant exfoliation of the carbon layers, causing the decline of microcrystalline in EG700 ºC [27].

The morphologies of FG_{100}, EG_{100}, and EG 700 ºC were observed by scanning electron microscopy, and the SEM images of the materials are exhibited in Figure 2. It can be seen that the original structure of the natural graphite is lamellar and layered (Figure 2a, a'). The graphite is made up of a stack of graphene sheets with compact interlayer spacing and there is virtually no observation of the boundary between the layers of the graphite. For expandable graphite, the material still exists in the same structure as the graphite (lamellar and layered) (Figure 2b, b'). However, there is a notable increase in the layer distance of EG, and the graphite is divided into units with a thickness of several hundred nanometers. Furthermore, the edges of EG are curled, and the bulging and spalling phenomena are observed obviously in Figure 2b'. These results are due to the oxidation process causing carbon bond fracture, which supports the intercalating compounds to move between graphene layers, resulting in the change of layer structure of the graphite. The results are consistent with the X-ray diffraction analysis mentioned above.

When exposed to heat, the fast evaporation of the blown gases (SO_2, CO_2, etc.), which are generated by the redox reaction between carbon and intercalation reagents (Scheme 1) [28] or the decomposition of oxygen-containing groups, produces the required pressure to break the weak Van der Waals bond between carbon layers and exfoliate those EG layers as a worm-like structure. Therefore, the layer distance of expanded graphite is extended remarkably. The expandable graphite is entirely transformed into expanded graphite with a volume hundreds of times larger than its original size (Figure 2c, c').

$$C + 2H_2SO_4 \longrightarrow CO_2 + H_2O + 2SO_2$$

Scheme 1. Redox reaction for blown gases responsible for the expansion of EG.

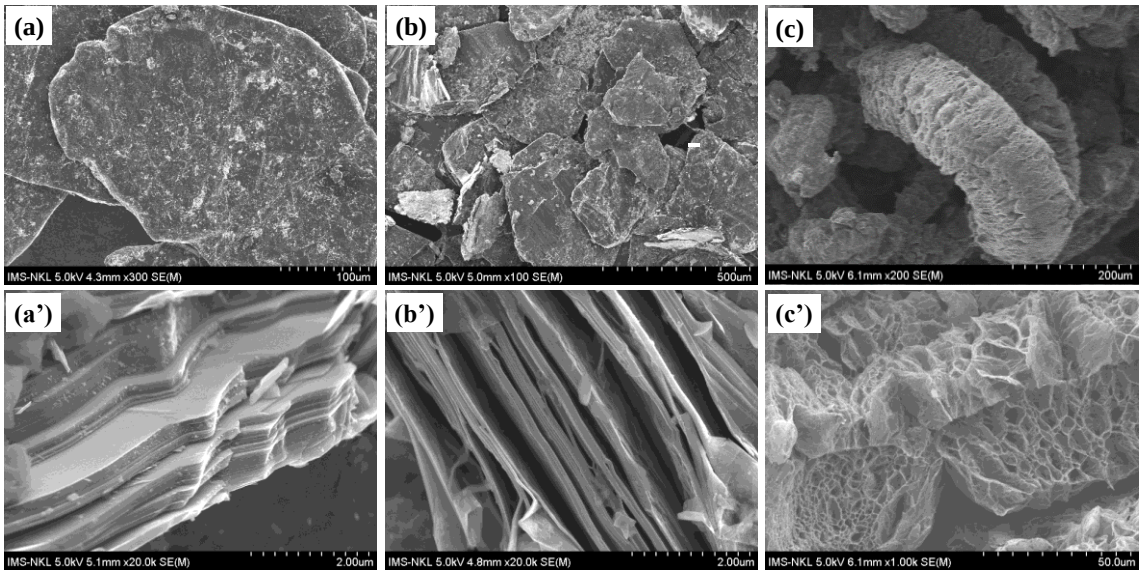

Figure 2. The morphology of FG_{100} (a, a'), EG_{100} (b, b'), and EG700ºC (c, c').

3.2. Effect of particle size on the expanded volume of expandable graphite

Expandable graphites EG_{50}, EG_{80}, EG_{100}, EG_{150}, and EG_{200} were synthesized under the same conditions using natural graphites with different particle sizes, including +50, +80, +100, +150, and +200 mesh, respectively. The expanded volume of expandable graphites was determined at various temperatures (200 - 700 ºC), and the results are shown in Figure 3.

Obviously, the initial expanded temperature of EG with bigger particle sizes (EG_{50}, EG_{80}, EG_{100}) (about 280 ºC) is much lower than that of EG with smaller particle sizes (EG_{150}, EG_{200}) (around 400 ºC), and it is opposite for the data of expanded volume. These results can be explained that the blown gases may easily escape from the edges of the small particles, thereby limiting the build-up of pressure needed inside the layers for sliding the graphene layers relative to one another. For the bigger particles, the retention of blown gases is more effective, and the necessary pressure to push the layers of graphite is promptly established before the gases may be escaped from the edges of the particles. On the other hand, there is an insignificant difference in the EV of EG_{50}, EG_{80}, and EG_{100} at temperatures below 500 ºC. However, the EV of EG_{100} increases considerably compared with others at above 500 ºC and reaches about 225 mL/g when thermal shocking at 700 ºC. For the larger graphite particles, namely +50 and +80 mesh, the

insertion of the intercalating reagents into interlayers is not deep enough, leading to the shortage of the compounds that may form propellants, resulting in the lack of force to exfoliate the carbon layers completely. For the particles with a medium size (+100 mesh), the necessary pressure to propel the carbon layers is lower than that of bigger particles. Therefore, the EV of EG_{100} is larger than EG_{50} and EG_{80}.

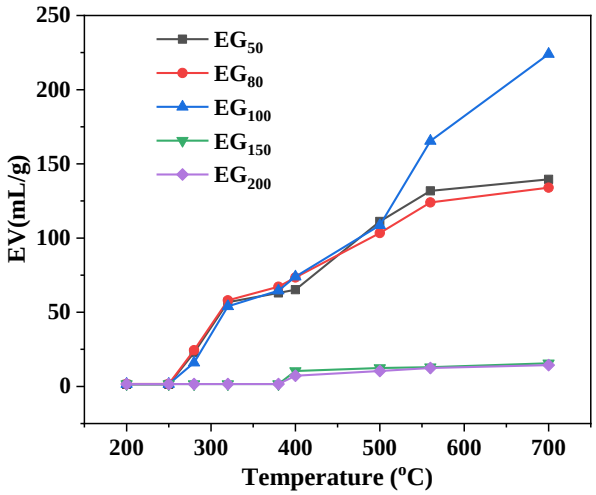

Figure 3. The expanded volume of expandable graphites at different temperatures.

In addition, the result of the EV measurement indicates that the EV of EG grows up upon the temperature increase. Specifically, the EV of EG_{100} rises sharply from 16 mL/g (at 280 ºC) to 225 mL/g (at 700 ºC). The exfoliation of EG is due to high temperature, leading to the phase transition to form pressure between the graphite layers to separate those layers. Because the expansion of EG is highly dependent on the repelling forces generated by blown gases, creating high pressure by using sudden and high temperatures can obtain a large expanded volume [15]. Heating slowly or at low temperatures lead to the building-up of a gas pressure lower than the necessary threshold to obtain maximum expansion. Consequently, the expanded volume of EG is low, even there is no expansion.

3.3. Flame retardant property

The flammability behaviors of neat PP and its flame-resistant composites were investigated by UL94-V and LOI tests, and the results are summarized in Table 2. Neat PP undergoes rapid combustion and produces a large amount of smoke in the UL94-V test with an LOI value of only 16.8 %. Adding a flame retardant such as EG, RP, or MC improves the flammability property of PP. The LOI values of PP1, PP2, and PP3 increase to 20 %, 21.5 %, and 23.7 %, with 18 wt.% of EG, RP, and MC, respectively. Significantly, the composite loading MC reaches the UL94 V-2 rating. The composites containing EG, RP, and MC at 1:1:1 of a mass ratio using the different size EGs also were prepared. It can be seen that the combination of these flame retardants causes a great improvement in the fire resistance of PP by the synergistic effect of EG, RP, and MC. Among the composites, the PP6 composite exhibits the greatest flame retardancy, which reaches the highest LOI of 28.9 %, and the vertical flame self-extinguished in shorter times after two ignitions, obtaining a UL94 V-0 rating. The result indicates that the flame resistance of the composite is proportional to the EV of expandable graphite.

Table 2. Flame retardant properties of the samples.

Sample code	UL94-V Rating	Phenomenon	LOI (%)
PP	No rating	Dripping, combustion up to holding clamp with high speed	16.8 ± 0.15
PP1	No rating	No dripping, combustion up to holding clamp with high speed	20 ± 0.2
PP2	No rating	Dripping, combustion up to holding clamp with low speed, smoky	21.5 ± 0.3
PP3	V-2	t_1 = 1s, t_2 = 31.2s, dripping, self-extinguishing	23.7 ± 0.1
PP4	V-2	t_1 = 1.15s, t_2 = 16.5s, dripping, self-extinguishing	25.9 ± 0.5
PP5	V-0	t_1 = 1.45s, t_2 = 1.25s, no dripping, self-extinguishing	26.8 ± 0.3
PP6	V-0	t_1 = 0.9s, t_2 = 0.8s, no dripping, self-extinguishing	28.9 ± 0.2
PP7	V-2	t_1 = 1.70s, t_2 = 25s, dripping, self-extinguishing	24.6 ± 0.2
PP8	V-2	t_1 = 2.09s, t_2 = 30.9s, dripping, self-extinguishing	24.1 ± 0.4

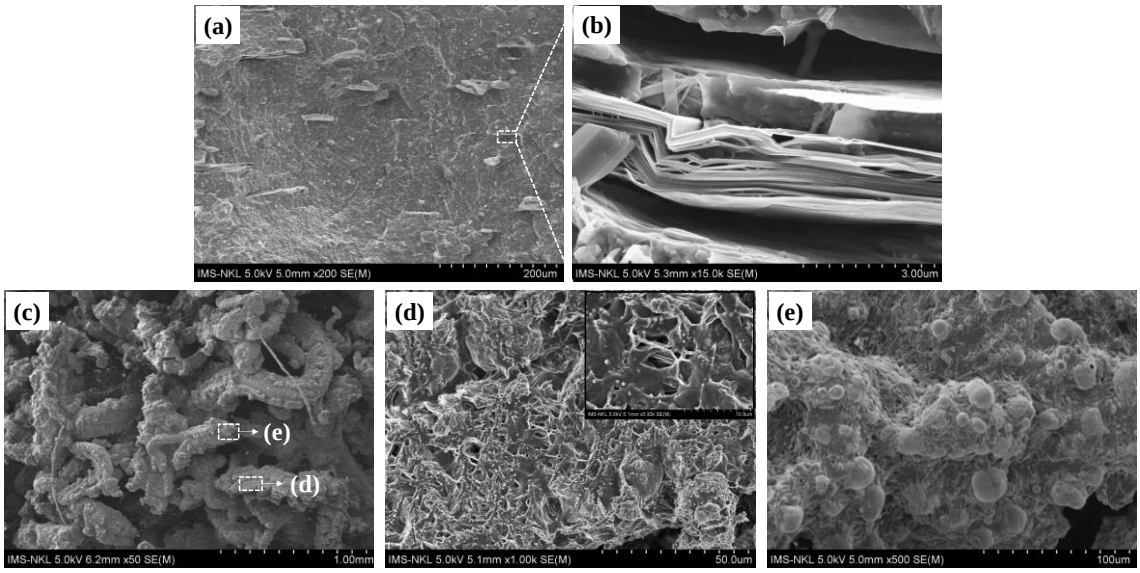

Figure 4. SEM images of the PP6 composite before (a, b) and after (c, d, e, and inset) the burning test.

Figure 4 illustrates the morphology of the PP6 composite before and after the vertical burning test. Obviously, EG exists in thin sheet structures inside the composite before heating (Figure 4a). The curly state of the edges of the expandable graphite can be observed in Figure

4b. After the vertical burning test, EG extends strongly into an insulating char layer with a large volume covering the surface of the burning material (Figure 4c). The swollen char layer acts as a thermal barrier in the condensed phase, preventing the heat transfer and the oxygen absorption to the interior composite and prolonging the release time of the volatile degradation products. The presence of RP and MC plays a role in reinforcing the char structure of expanded graphite. RP and MC can cause N-P synergistic effects in the burning process, which is the interaction between P-containing and N-containing flame retardants generating macromolecular compounds ($(PNO)_x$ or $(PN)_x$) with high viscosity and thermal stability covering the surface of the expanded graphite (Figure 4d, e, and inset). As a result, a thicker and more compact char layer is formed, and the condensed phase flame retardant mechanism of the composite becomes more effective.

3.4. Thermo-oxidative stability

The synergism of EG, RP, and MC on the thermo-oxidative stability of PP was also investigated by thermal gravimetric analysis. The TGA and DTG thermograms of the samples under air are depicted in Figures 5a and 5b, respectively. Additionally, the TGA parameters, consisting of temperatures at 5 % mass loss ($T_{5\%}$), maximum mass loss temperature (T_{max}), and char residue (remaining residue percentage at 500 ºC and 900 ºC), are represented in Table 3. The neat PP is completely degraded at 553 ºC, and its char yield is acquired at 0.33 wt.% at 900 ºC. The $T_{5\%}$ and T_{max} values of neat PP are about 287 ºC and 424 ºC, respectively. With adding 18 wt.% EG, the $T_{5\%}$ value of PP decreases to 281.7 ºC due to the release of the blown gasses (CO_2, SO_2, and H_2O). Also, the T_{max} of the composite is shifted about 36 ºC to a lower temperature than neat PP. The worm-like structure of the expanded graphite formed by the thermal expansion along the *c*-axis of the expandable graphite can store the gaseous products of the PP decomposition. As a consequence, the lifetime of the free radicals is prolonged, which can accelerate the thermo-oxidation of PP [29]. At 500 ºC, the char yield of the PP1 composite is 18.67 wt.%, but the char oxidation occurs with the increase in temperature, resulting in an 86.88 % reduction of char residue at 900 ºC. For the PP2 composite, the $T_{5\%}$ and T_{max} rise dramatically by 36.4 ºC and 26 ºC in comparison with neat PP, respectively. These results are owing to the formation of a film layer of phosphoric acid or polyphosphoric covering on the surface of the burning material by the thermal oxidation of red phosphorus in the condensed phase [30, 31], which can restrict the heat and mass transition, thereby suppressing the thermal decomposition of PP. In the case of PP3, the endothermic degradation of melamine cyanurate generates the condensation polymers consisting of melam, melem, and melom [32], leading to the remarkable increment of the char residue below 500 ºC (about 23.3 wt.%). Furthermore, the endothermic process of MC also slows down the thermal decomposition rate of the composite. Thus the T_{max} of the composite shifts slightly to a higher temperature by 6.5º compared with neat PP. However, the condensation polymers are degraded at higher temperatures, and the composite loading MC of 18 wt% only leaves little residue at 900 ºC (1.46 wt.%).

The residue contents of the PP6 composite at 500 ºC and 900 ºC are 20.64 and 6.85 wt.%, which are more extensive than that of $PP6_{calculated}$ (17.66 and 4.53 wt.%, respectively). Moreover, the T_{max} value of this system is higher than that of PP without fillers by 15.7 ºC. These results evince that the incorporation of EG, RP, and MC improves the thermo-oxidative stability of PP. The explanation can be the interaction between RP and MC forming macromolecules such as $(PNO)_x$ and $(PN)_x$ with high thermal stability, which can cover the surface of expanded graphite. Thus, the contact between expanded graphite and oxygen is reduced, which positively affects the retention of expanded graphite.

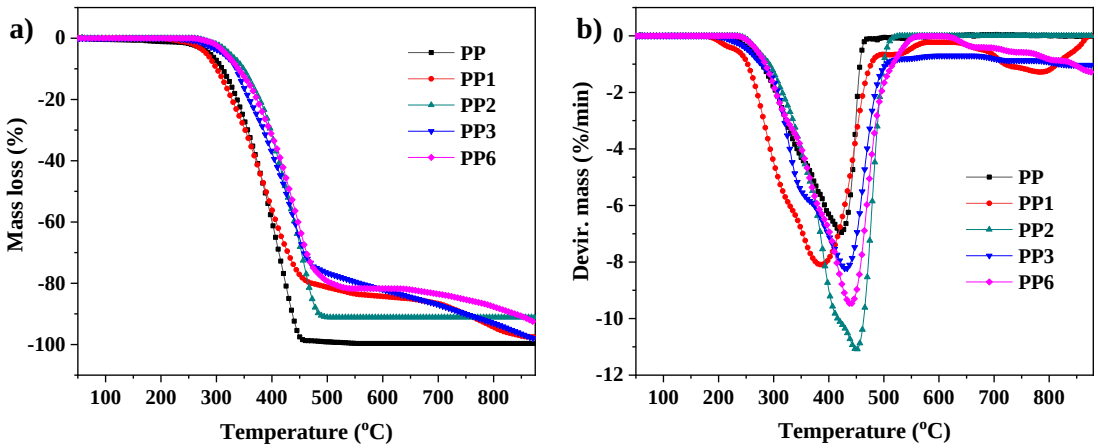

Figure 5. TGA (a) and DTG (b) curves of neat PP and its composites under air.

Table 3. The results of TGA analysis in air.

Sample code	$T_{5\%}$ (°C)	T_{max} (°C)	Char residue (wt.%)	
			500 °C	900 °C
PP	287	424	0.86	0.33
PP1	281.7	388	18.67	2.45
PP2	323.4	450	8.91	8.88
PP3	313	430.5	23.3	1.46
PP6	316.5	439.7	20.64	6.85
$PP6_{calculated}$	-	-	17.66	4.53

3.5. Mechanical properties

Table 4 presents the tensile strength, elongation at break, and Izod unnotched impact strength of PP and its flame retardant composites. It can be seen that the composites manifest a deterioration in the mechanical properties compared to neat PP. The tensile strength and elongation at break of the composite loading 18 wt.% EG_{100} (PP1) are reduced greater than others, which decrease by 22.69 % and 62.24% compared with neat PP, respectively. This is caused by the incompatibility and the big size of EG, leading to the formation of defects in the composite and the poor adhesion between EG particles and the PP matrix [33, 34]. However, the MC additive significantly affects the Izod impact strength of PP. The impact strength falls sharply from 55.36 kJ/m^2 (PP) to 8.5 kJ/m^2 (PP3), corresponding to 84.65 %, due to the rigid structure of MC. The effect of different particle sizes of EG on the mechanical properties is also evaluated. It is clear that the increase in particle size of EG deteriorates the mechanical properties of the composites. The tensile strength, elongation, and impact strength of the composite loading EG_{50} are 26.35 MPa, 25.68 %, and 13 kJ/m^2, which drop by 8.44 %, 30.31 %, and 48.84 % in comparison with the composite loading EG_{200}, respectively.

In order to explain these results of the mechanical measurements, the fracture surfaces of the composites were investigated, and Figure 6 depicts the SEM images of PP5, PP6, and PP8. It can be observed that EG particles are distinct in the matrix, and there are gaps in the phase interfaces, indicating the poor compatibility of the material with the PP matrix. Furthermore, the gaps are observed more obviously in the composites containing bigger particle size EGs. These phenomena can explain the decrease in the mechanical properties of the composites when particle sizes of EG increase. In addition, the good cohesion and dispersion of RP and MC

treated with poly(methyl-hydro siloxane) are shown in Figure 6. There are almost no observation of defects between RP and MC particles and the polymer matrix, proving that the compatibility of these additives is notably improved after modifying with the silane agent. As a result, the bad influence of these fillers on the mechanical properties of the composites is mitigated.

Table 4. Mechanical properties of the samples.

Sample code	Tensile strength (MPa)	Elongation at break (%)	Izod impact strength (kJ/m^2)
PP	32.97 ± 1.35	62.16 ± 5.0	55.36 ± 1.5
PP1	25.49 ± 1.32	23.47 ± 4.0	14.10 ± 0.1
PP2	29.06 ± 0.75	45.75 ± 4.5	15.68 ± 0.15
PP3	32.74 ± 0.30	31.15 ± 5.5	8.5 ± 0.24
PP4	26.35 ± 1.05	25.68 ± 3.5	13.0 ± 0.35
PP5	26.96 ± 0.55	29.05 ± 3.0	16.46 ± 0.20
PP6	27.58 ± 0.85	33.15 ± 2.0	21.52 ± 0.13
PP7	28.02 ± 1.2	35.40 ± 5.0	27.82 ± 0.50
PP8	28.78 ± 0.92	36.85 ± 2.5	25.40 ± 0.30

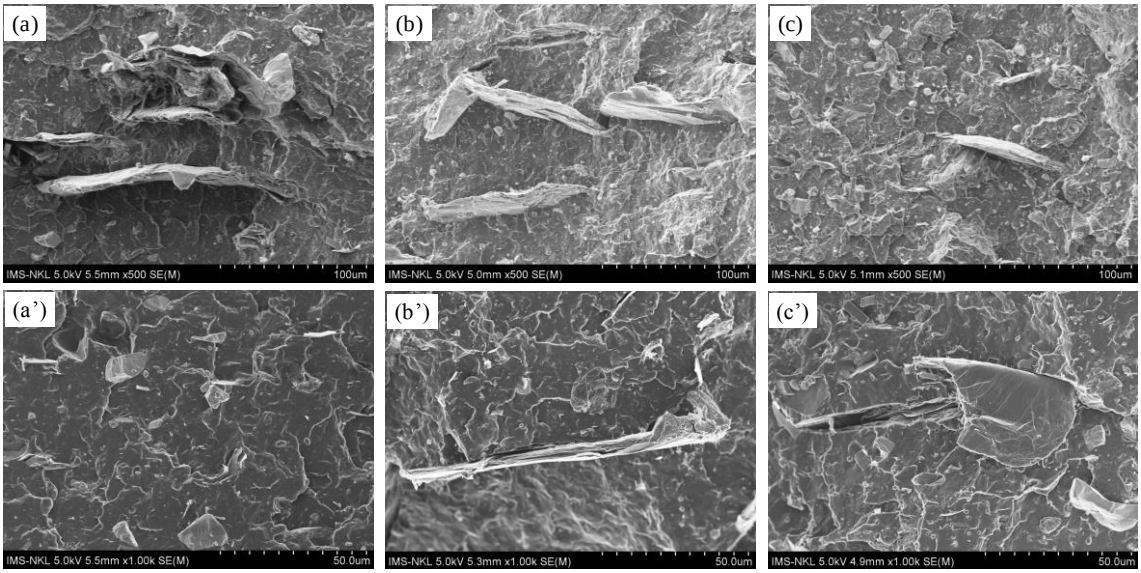

Figure 6. The fracture surfaces of PP5 (a, a'), PP6 (b, b'), and PP8 (c, c').

4. CONCLUSIONS

In this work, the expandable graphites with various particle sizes were successfully prepared by the chemically oxidative intercalation method employing flaky graphites (+50, +80, +100, +150, and +200 mesh) as raw materials, $KMnO_4$ as an oxidant, NH_4NO_3 as an

intercalation-assisted reagent, and concentrated H_2SO_4 as both an intercalation reagent and the environment for the oxidative reaction. EG_{100} shows the greatest exfoliation volume (225 mL/g) with a low initial expanded temperature (about 280 ºC). Synergism between EG, RP, and MC on the flame retardancy and thermo-oxidation property of PP is found because of the formation of macromolecules such as $(PNO)_x$ and $(PN)_x$ produced by the interaction between RP and MC protecting the char structure of expanded graphite. The composite containing EG_{100}, RP, and MC exhibits the most flame resistance efficiency with the LOI value of 28.9 % and UL94 V-0 rating. The product EG_{100}, with low initial expansion temperature and high expanded volume, shows great potential for applications as a flame retardant.

Acknowledgements. This research was funded by the Institute of Chemistry under grant number VHH.2022.04. Hac Thi Nhung acknowledges the financial support from the PhD Scholarship Programme of Vingroup Innovation Foundation (Code VINIF.2022.TS.089).

CRediT authorship contribution statement. Nhung Hac Thi, Thi Thu Hien Nguyen, Truong Cong Doanh: Methodology, Investigation. Do Thi Mai Huong, Tien Dat Doan, Ho Thi Oanh, Nguyen Duc Tuyen: Formal analysis. Nhung Hac Thi: Writing - original draft. Mai Ha Hoang: Supervision, review & editing.

Declaration of competing interest. The authors declare that they have no known competing financial interests or personal relationships that could have appeared to influence the work reported in this paper.

REFERENCES

1. Lin S., Dong L., Zhang J., Lu H. - Room-Temperature Intercalation and 1000-Fold Chemical Expansion for Scalable Preparation of High-Quality Graphene, Chem. Mater. **28** (2016) 2138-2146. doi.org/10.1021/acs.chemmater.5b05043
2. Tang Y., Peng P., Wang S., Liu Z., Zu X., Yu Q. - Continuous Production of Graphite Nanosheets by Bubbling Chemical Vapor Deposition Using Molten Copper, Chem. Mater. **29** (2017) 8404-8411. doi.org/10.1021/acs.chemmater.7b02958
3. Zhan H., Zhang Y., Bell J. M., Gu Y. - Suppressed Thermal Conductivity of Bilayer Graphene with Vacancy-Initiated Linkages,J. Phys. Chem. C**119** (2015) 1748-1752. doi.org/10.1021/jp5117905
4. Wang H., Wei C., Zhu K., Zhang Y., Gong C., Guo J., Zhang J., Yu L., Zhang J. - Preparation of Graphene Sheets by Electrochemical Exfoliation of Graphite in Confined Space and Their Application in Transparent Conductive Films,ACS Appl. Mater. Interfaces **9** (2017) 34456-34466. doi.org/10.1021/acsami.7b09891
5. Cheng X., Li G., Yu G., Li Y., Han J. - Effect of expanded graphite and carbon nanotubes on the thermal performance of stearic acid phase change materials,J. Mater. Sci.**52** (2017) 12370-12379.
6. Xu T., Li Y., Chen J., Liu J. - Preparation and thermal energy storage properties of LiNO3-KCl-NaNO3/expanded graphite composite phase change material, Sol. Energy Mater. Sol. Cells **169** (2017) 215-221. doi.org/10.1016/j.solmat.2017.05.035
7. Chen L., Wang Y. Z. - A review on flame retardant technology in China. Part I: development of flame retardants, Polym. Adv. Technol. **21** (2010) 1-26. doi.org/10.1002/pat.1550
8. Duquesne S., Bras M. L., Bourbigot S., Delobel R., Vezin H., Camino G., Eling B., Lindsay C., Roels T. - Expandable graphite: a fire retardant additive for polyurethane coatings, Fire Mater. **27** (2003) 103-117. doi.org/10.1002/fam.812

9. Dresselhaus M. S., Dresselhaus G. - Intercalation compounds of graphite. Adv. Phys. **30** (1981) 139-326. doi.org/10.1080/00018738100101367
10. Shin Y. R., Jung S. M., Jeon I. Y., Baek J. B. - The oxidation mechanism of highly ordered pyrolytic graphite in a nitric acid/sulfuric acid mixture, Carbon **52** (2013) 493-498. doi.org/10.1016/j.carbon.2012.10.001
11. Focke W. W., Badenhorst H., Mhike W., Kruger H. J., Lombaard D. - Characterization of commercial expandable graphite fire retardants, Thermochim. Acta **584** (2014) 8-16. doi.org/10.1016/j.tca.2014.03.021
12. Kovtyukhova N. I., Wang Y., Berkdemir A., Cruz-Silva R., Terrones M., Crespi V. H., Mallouk T. E. - Non-oxidative intercalation and exfoliation of graphite by Brønsted acids, Nat. Chem. **6** (2014) 957-973. doi.org/10.1038/nchem.2054
13. Hong X., Chung D. D. L. - Exfoliated graphite with relative dielectric constant reaching 360, obtained by exfoliation of acidintercalated graphite flakes without subsequent removal of the residual acidity, Carbon **91** (2015) 1-10. doi.org/10.1016/ j.carbon.2015.04.042
14. Yuan Y., Yang H., Yu B., Shi Y., Wang W., Song L., Hu Y., Zhang Y. - Phosphorus and nitrogen-containing polyols: synergistic effect on the thermal property and flame retardancy of rigid polyurethane foam composites, Ind. Eng. Chem. Res. **55** (2016) 10813-10822. doi.org/10.1021/acs.iecr.6b02942
15. Chung D. D. L. - A review of exfoliated graphite, J. Mater. Sci. **51** (2016) 554-568. doi.org/10.1007/s10853-015-9284-6
16. Sorokina N. E., Maksimova N. V., Nikitin A. V., Shornikova O. N., Avdeev V. V. - Synthesis of intercalation compounds in the graphite−HNO3−H3PO4 system. Inorg. Mater. **37** (2001) 584-590. doi.org/10.1023/A:1017512216205
17. Saidaminov M. I., Maksimova N. V., Zatonskih P. V., Komarov A. D., Lutfullin M. A., Sorokina N. E., Avdeev V. V. - Thermal decomposition of graphite nitrate, Carbon **59** (2013) 337-343. doi.org/10.1016/j.carbon.2013.03.028
18. Li J., Li J. H., Li M. - Ultrasound irradiation prepare sulfur-free and lower exfoliate-temperature expandable graphite, Mater. Lett. **62** (2008) 2047-2049. doi.org/10.1016/ j.matlet.2007.11.011
19. Wei X. H., Liu L., Zhang J. X., Shi J. L., Guo Q. G. - The preparation and morphology characteristics of exfoliated graphite derived from HClO4-graphite intercalation compounds, Mater. Lett. **64** (2010) 1007-1009. doi.org/10.1016/j.matlet.2009.11.025
20. Yu X. J., Wu J., Zhao Q., Cheng X. W. - Preparation and characterization of sulfur-free exfoliated graphite with large exfoliated volume, Mater. Lett. **73** (2012) 11-13. doi.org/10.1016/j.matlet.2011.11.078
21. Zhao Q., Cheng X. W., Wu J., Yu X. J. - Sulfur-free exfoliated graphite with large exfoliated volume: Preparation, characterization and its adsorption performance, J. Ind. Eng. Chem. **20** (2014) 4028-4032. doi.org/10.1016/j.jiec.2014.01.002
22. Saidaminov M. I., Maksimova N. V., Kuznetsov N. G., Sorokina N. E., Avdeev V. V. - Fire protection performance of oxidized graphite modified with boric acid, Inorg. Mater. **48** (2012) 258-262. doi.org/10.1134/S0020168512030132
23. Asghar H. M. A., Hussain S. N., Sattar H., Brown N. W., Roberts E. P. L. - Environmentally friendly preparation of exfoliated graphite, J. Ind. Eng. Chem. **20** (2014) 1936-1941. doi.org/10.1016/j.jiec.2013.09.014

24. Chung D. D. L. - Review graphite, J. Mater. Sci. **37** (2002) 1475-1489. doi.org/10.1023/A:1014915307738
25. Kuan C. F., Tsai K. C., Chen C. H., Kuan H. C, Liu T. Y., Chiang C. L. - Preparation of Expandable Graphite via H2O2-Hydrothermal Process and Its Effect on Properties of High-Density Polyethylene Composites, Polym. Compos. **33** (6) (2012) 872-880. doi.org/10.1002/pc.22224
26. Sharma N., Vyas R., Sharma V., Rahman H., Sharma S. K., Sachdev K. - A comparative study on gas-sensing behavior of reduced graphene oxide (rGO) synthesized by chemical and environment-friendly green method, Appl Nanosci **10** (2020) 517-528. doi.org/10.1007/s13204-019-01138-7
27. Zu C., Li L., Qie L., Manthiram A. - Expandable-graphite-derived graphene for next-generation battery chemistries, J. Power Sources **284** (2015) 60-67. doi.org/10.1016/j.jpowsour.2015.03.009
28. Camino G., Duquesne S., Delobel R., Eling B., Lindsay C., Roels T. - Mechanism of expandable graphite fire retardant action in polyurethanes, in: Fire and Polymers, American Chemical Society, Chapter 8 (2001) 90-109.
29. Wang G., Bai S. - Synergistic effect of expandable graphite and melamine phosphate on flame-retardant polystyrene, J. Appl. Polym. Sci., **134** (2017) 45474. doi.org/10.1002/app.45474
30. Thi N. H., Nguyen T. N., Oanh H. T., Trang N. T. T., Tham D. Q., Nguyen H. T., Van Nguyen T., Hoang M.H. - Synergistic effects of aluminum hydroxide, red phosphorus, and expandable graphite on the flame retardancy and thermal stability of polyethylene, J. Appl. Polym. Sci. **138** (17) (2021) 50317. doi.org/10.1002/app.50317.
31. Si G., Li D., You Y., Hu X. - Investigation of the influence of red phosphorus, expansible graphite and zinc borate on flame retardancy and wear performance of glass fiber reinforced PA6 composites, Polym. Compos. **38** (10) (2015) 2090-2097. doi.org/10.1002/pc.23781.
32. Modesti M., Lorenzetti A. - Flame retardancy of polyisocyanurate–polyurethane foams: use of different charring agents, Polym. Degrad. Stab.**78** (2) (2002) 341-347. doi.org/10.1016/S0141-3910(02)00184-2
33. Liu Y. L., He J. Y., Yang R. J. - Effects of dimethylmethylphosphonate, aluminum hydroxide, ammonium polyphosphate,and expandable graphite on the flame retardancy and thermalproperties of polyisocyanurate−polyurethane Foams. Ind. Eng. Chem. Res. **54** (2015) 5876-5884. doi.org/10.1021/acs.iecr.5b01019
34. Wang B. B., Hu S., Zhao K. M., Lu H. D., Song L., Hu Y. - Preparation of polyurethane microencapsulated expandable graphite,and its application in ethylene vinyl acetate copolymer containingsilica-gel microencapsulated ammonium polyphosphate, Ind. Eng. Chem. Res. **50** (2011) 11476-11484. doi.org/10.1021/ie200886e.